Materials and Design 160 (2018) 363–370

Contents lists available at ScienceDirect

Materials and Design

journal homepage: www.elsevier.com/locate/matdes

Thermographic investigation of strain rate effects in Al foams and Ni/Al hybrid foams

A. Jung[a,*], S. Bronder[a], S. Diebels[a], M. Schmidt[b], S. Seelecke[b]

[a] Saarland University, Applied Mechanics, Campus A4.2, Saarbrücken 66123, Germany
[b] Saarland University, Multifunctional Materials Systems Lab, P.O. Box 151150, 66041 Saarbrücken, Germany

HIGHLIGHTS

- Investigation of Al and Ni/Al foams by infrared thermography shows increasing heat evolution with increasing strain rate
- First time synchronisation of digital image correlation and infrared thermography applied to foams with good correlation
- Fully-coupled thermomechanical analysis led to a better understanding of the micromechanical deformation mechanism
- Increasing nickel coating thickness causes increase in heat evolution during plastic deformation

GRAPHICAL ABSTRACT

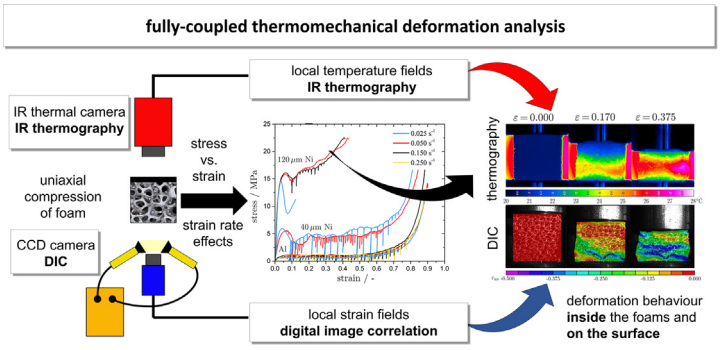

ARTICLE INFO

Article history:
Received 30 June 2018
Received in revised form 3 September 2018
Accepted 10 September 2018
Available online 16 September 2018

Keywords:
Open-cell metal foams
Ni/Al hybrid foams
Digital image correlation
Thermography
Deformation analysis

ABSTRACT

Open-cell metal foams are biomimetic open-porous materials mimicking the construction elements of bones. Based on their special porous microstructure, they are used as lightweight construction elements and for crash energy absorbers. Ni/Al hybrid foams are aluminium (Al) foams electrochemically coated with nanocrystalline nickel (Ni) leading to enhanced strength and energy absorption capacity. A robust understanding and knowledge of the deformation behaviour under different strain rates are essential to design crash absorbers made of foams. The present contribution is focused on the investigation of strain rate effects and is furthermore a pioneering work dealing with a full thermomechanical characterisation of the deformation behaviour in Al foams and Ni/Al hybrid foams by a combination of digital image correlation for measuring local strain fields and infrared thermography for measuring local temperature fields during the deformation process.

1. Introduction

Open-cell foams are an interesting, novel class of bio-inspired porous materials, which mimic natural lightweight materials such as femur bones [1]. Foams offer a 3D porous network of stochastically distributed interconnected pores and show a great potential for application as lightweight construction elements and crash energy absorbers [2,3].

Ni/Al hybrid foams are a special class of composite foams consisting of aluminium foams electrochemically coated with a nanocrystalline layer of nickel [4-8]. Such hybrid foams offer superior mechanical properties such as high strength and large energy absorption capacity compared to conventional open-cell metal foams. Further hybrid foams are based on Cu/Al hybrid foams [9-11] and Ni/polyurethane hybrid foams [12].

* Corresponding author.
E-mail address: anne.jung@mx.uni-saarland.de (A. Jung).

https://doi.org/10.1016/j.matdes.2018.09.020
0264-1275/

The development of new materials and structures for structural design, energy absorption and seismic applications requires a comprehensive characterisation of there properties. In experimental mechanics, material properties are characterised at different mechanical load cases like tension, compression, torsion and shear. Within these experiments, measurement values like stress and strain are acquired to identify the material properties. Based on these measurements material models can be developed to predict the mechanical behaviour of complex structures at different load cases. Extensometers, laser tracing, edge detection and strain gauges are typically used to determine global deformations, whereas digital image correlation (DIC) is applied to describe local strain fields. All of these methods are associated with the measurement of dimensional changes between two points on the specimen or smaller regions on the specimen [13]. The above-mentioned measurement methods are suitable for a comprehensive description of the quasi-static mechanical behaviour of materials. However, elastic and plastic deformations are accompanied by heat energy dissipation, which can only be captured by thermal measurement methods. Plastic deformations at high strain rates lead to a significant temperature change in the specimen, in some materials also affecting their mechanical behaviour. The visualisation of the heat evolution during deformation enables the observation of plastification in materials. A suitable method to capture temperature distributions in high dynamic processes is infrared (IR) thermography. This technology is established in failure and deformation process analysis inside and on the surface of components and structures [14]. A further field of application is the characterisation of smart materials like shape memory alloys [15-18].

All types of deformations in a material cause heat dissipation but the heat production for plastic deformations is about one order of magnitude larger than that for elastic deformations [13]. The observable temperature change depends largely on the thermal conductivity λ of the investigated material and on the applied deformation rate.

Also Ni/Al hybrid foams show excellent energy absorption characteristics as well as a rate dependent temperature development. In these materials deformation processes under high strain rates result in an adiabatic heating. Consequently, dynamic deformations cause very large temperature increases, since there is not enough time for heat conduction [13]. The temperature change ΔT during an elasto-plastic deformation of a material subjected to uniaxial stress σ is given by [19,20],

$$\Delta T\left(\varepsilon^{p}\right)=\frac{\eta}{\rho\, c_{v}}\int_{0}^{\varepsilon^{p}}\sigma\left(\varepsilon^{p},\,\dot{\varepsilon},\,T\right)\,\mathrm{d}\varepsilon^{p}, \tag{1}$$

where ε^{p} belongs to the plastic strain, and η is the fraction of plastic work converted into heat. In the case of metals, η is usually supposed to be a constant parameter of 0.9. c_v is the heat capacity at constant volume, since plastic flow is isochoric. $\dot{\varepsilon}$ denotes to the strain rate, ρ is the density of the material and T describes the actual temperature. On the one hand, the lower the strain rate, the lower is the heat evolution. On the other hand, the higher the thermal conductivity of the investigated material the more difficult it is to use IR thermography due to temperature changes based on heat conduction. With respect to the investigation of Al foams and Ni/Al hybrid foams, the thermal conductivity for $AlSi_7Mg_{0.3}$ is about $\lambda_{Al} = 150 - 180$ W m^{-1} K^{-1} [21], while it is $\lambda_{Ni} \approx 95$ W m^{-1} K^{-1} for nickel [22,23]. Nickel should provide larger temperature increase under plastic deformation than aluminium because of the twice as large thermal conductivity of aluminium. The density of nickel is about three times larger than that of aluminium ($\rho_{Ni} = 8.91$ g cm^{-3}, $\rho_{Al} = 2.66$ g cm^{-3}), while the heat capacity is about half as large as that of aluminium ($c_{v,Ni} = 0.444$ J kg^{-1} K^{-1}, $c_{v,Al} = 0.896$ J kg^{-1} K^{-1}). Hence, resulting from Eq. (1), aluminium should provide a 1.66 times larger temperature increase than nickel.

Thermographic investigations of homogeneous specimens made of pure aluminium and $AlSi_7Mg$ alloys, respectively, were performed by Krstulović-Opara et al. [13] and Wagner et al. [24]. Wagner et al. [24] studied the fatigue crack initiation detection by an infrared thermography method and concluded from their results that IR thermography is suitable for the indirect visualisation of irreversible deformation and plastification in aluminium alloys and for the investigation of failure evolution and crack propagation when applying a mechanical load. Krstulović-Opara et al. [13] were the first to compare IR thermography and DIC. Both methods can be used to study plastic deformation processes but they are based on the measurement of different physical properties, temperature versus strain. In general, DIC is limited by the necessary illumination under high strain rates and the high frame rates, which must be supported by the used camera. IR thermography is limited by the heat conduction under lower strain rates [13]. Although DIC is successfully used in recent studies for the mechanical characterisation of material in general and even foams under high impact loading (e.g. [25-27]), based on the requirements, DIC is superior for mechanical characterisation using low strain rates, whereas IR thermography has advantages for investigations under dynamic loading. Both methods have their limitations. However these can be overcome by a combination of the methods using the advantages of each method. Especially a combination of DIC and IR thermography is a powerful method for comprehensive characterisation of complex material behaviour and is required for the development of thermomechanically coupled material models [28,29]. Further, Krstulović-Opara et al. [13] stated that the heat generated during the deformation process represents the plastic strain in the material.

A common application of IR thermography related to foams is the monitoring of the exothermic foaming process of closed-cell foams [30]. However, IR thermography has also already been used in a handful of publications on the investigation of the deformation mechanisms in foams. First, Clarke et al. [31] used thermographic images for void detection in polyurethane foams. In 2010, Crupi et al. [32] applied IR thermography for the investigation of failure modes and damage evolution in PVC and Al sandwich panels under drop weight loading and compared the results with 3D CT measurements. Wang et al. [33] studied the deformation in PVC foam sandwich panels under three-point bending. Most other work subjected to IR thermography and foams was conducted by Vesenjak et al. [34,35]. They studied the deformation process of aluminium foams with and without silicone filling under quasi-static and dynamic loading [34] and conducted an experimental as well as a numerical study to gain insight into the deformation behaviour of aluminium foams under dynamic compression [35]. Further work on the static and dynamic behaviour of foam-filled tubes can be found by Duarte et al. [36-38]. A detailed overview of the use of IR thermography as a method for energy absorption evaluation of metal foams is given by Krstulović-Opara et al. [39].

The present contribution deals with the investigation of the applicability and limitations of a combination of DIC and IR thermography to study the deformation and failure behaviour of conventional open-cell Al foams and new Ni/Al hybrid foams. Strain rate effects on the mechanical properties and on the heat evolution during plastic deformation as well as the effect of the coating thickness in the Ni/Al hybrid foams is studied. The present study is the pioneering work dealing with a full thermomechanical characterisation of the deformation behaviour in foams and hybrid foams by a coupling of DIC for measuring local strain fields and IR thermography for measuring local temperature fields to gain deeper insight on the plastic deformation mechanism.

2. Materials and methods

2.1. Aluminium alloy foams and hybrid foams

Cubic aluminium (Al) alloy foams ($AlSi_7Mg_{0.3}$, $20\times20\times20\,mm^3$) with a pore size of 20 ppi were purchased from Celltec Materials GmbH, Dresden, Germany. Ni/Al hybrid foams were produced from the Al foams by coating these Al foams with various coating thicknesses of 40 μm and 120 μm of hard facing nickel (Ni) using electrodeposition [6,8].

2.2. Experimental setup

Al foams and Ni/Al hybrid foams were analysed in uniaxial compression tests under displacement control using an ElectroPuls^{TM} E10000 universal testing machine of Ltd. Instron, Pfungstadt, Germany equipped with a ±10 kN and ±100 Nm Dynacell load sensor. Initial strain rates ranging from $0.025\,s^{-1}$ to $0.250\,s^{-1}$ were applied to check for strain rate effects. The specific tests were performed three times for each specimen type and strain rate for better statistics. A coupling between DIC for measuring local strains and IR thermography for measuring local temperatures was needed for the performance of a full thermomechanical characterisation. Thus, the experiments were simultaneously monitored by a CCD camera (Marlin F-131C, Ltd. Allied Vision Technologies, Stadtroda, Germany) for DIC and a cooled high-performance middle-wave IR thermal camera. A high resolution IR camera system (ImageIR9360, Infratec GmbH, Dresden, Germany) with a detector size of 1280×1024 pixels was used for temperature distribution measurements of the Al foams and the Ni/Al hybrid forms. The InSb detector operates at a spectral range between 3 and 5 μm. The system has a frame rate of up to 3.2 kHz in sub-frame mode and 100 Hz in full frame mode. When using a 50 mm objective with close-up lens a pixel size of the 60 μm can be achieved, whereas small scale effects can be investigated with a microscope lens which provides a minimum pixel size of 15 μm. The tests were performed with a thermal resolution of 0.02 °C. The IR camera was synchronised with the DIC camera by an external trigger signal from the universal testing machine. The setup is shown in Fig. 1.

Both investigation methods need special requirements for conclusive measurement data. The DIC needs proper illumination of the specimen and a random speckle pattern, while IR thermography needs dull and dark surfaces for proper calibration of the thermal camera and the prevention of errors due to light reflections. Hence, the foam specimens were surrounded by a box, which was painted inside with black camera varnish having a thermal emissivity coefficient of 0.97 (no. 105202, TETENAL Europe GmbH, Norderstedt, Germany). The box had two facing open windows for the observation with the CCD and the IR thermal camera. Further, also the foams were painted on the side facing the IR thermal camera with a thin layer of the black camera varnish to guarantee conclusive results of the thermographic measurements. Whereas light can cause errors in IR thermography, it is indispensable for DIC. Since the motivation of the work is to study macroscopic deformation behaviour, the natural mesostructure of the foams was used as speckle pattern. This offers the possibility to investigate features in the deformation process, which are at least of equal size as a pore. Local deformation processes on the mesoscale such as strut buckling (see e.g. [40,41]) cannot be detected by using the mesostructure of the foams as natural speckle pattern. In order to guarantee sufficient light for good quality image correlation, the foams were not centred in the black box, but placed near the open window facing to the CCD camera. A cold-light source emitting light with a significantly reduced fraction of IR radiation provided a good illumination from the side of the CCD camera.

The images from the CCD camera were analysed by DIC using the commercial software Vic2D® from Ltd. Correlated Solutions, Columbia, USA for the pattern matching and the calculation of the strains in loading direction ε_{yy}. In contrast to Vic3D®, Vic2D® only allows for in-plane surface measurements and not for out-of-plane analysis. Since in highly porous structures, the magnitude of out-of-plane displacement is negligible, a 2D analysis using only a one camera setup is sufficient for the evaluation of the experiments. The thermographic images were analysed by the commercial software IRBIS®3 from Infratec GmbH, Dresden, Germany. Since the CCD camera and the IR thermal camera were face to face, the DIC images were mirrored vertically to obtain corresponding 2D full-field maps of local temperature and local strain of the specimens.

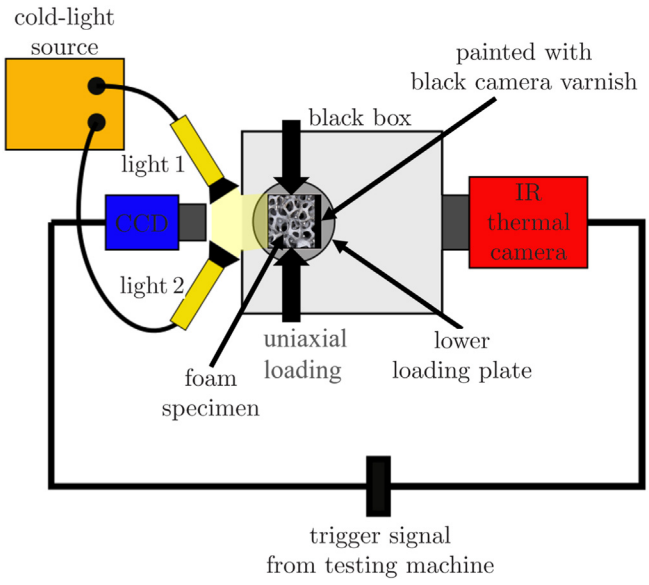

Fig. 1. Experimental setup for the full thermomechanical analysis simultaneously using DIC and IR thermography.

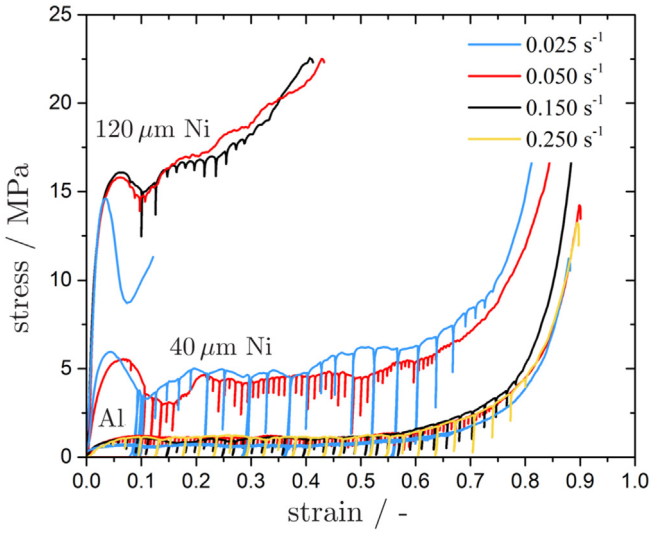

Fig. 2. Engineering stress-strain curves of Al foams and Ni/Al foams for different strain rates. (For reasons of clarity, only one representative curve per test and specimen type is shown.)

3. Results and discussion

3.1. Thermographic analysis of strain rate effects

Fig. 2 presents the stress-strain behaviour of Al foams and Ni/Al hybrid foams for strain rates ranging from $0.050\,s^{-1}$ to $0.250\,s^{-1}$. Unfortunately, due to the different stiffnesses, with the used all-electric Instron ElectroPlus^{TM} E10000 universal testing machine it was not possible to perform the uniaxial compression tests on all specimens with all four strain rates. Nevertheless, as already expected from previous work [25], for the investigated Al foams and Ni/Al hybrid foams there is no strain rate-dependent behaviour in this strain rate regime visible in the stress-strain response. The slight variations for the individual types are caused by variations in the density and the mesostructure. The Ni/Al hybrid foams with a coating thickness of 40 μm nickel provide about five times higher plastic collapse stress (PCS) and plateau stress than the pure Al alloy foams as a result of the strengthening by the nickel coating. A coating thickness of 120 μm nickel leads to an increase of PCS by a factor of about 15 along with a reduction in the densification strain.

Fig. 3 depicts thermographic images of the compressive loading sequence of Al foams for the four investigated strain rates. The thermograms for $\varepsilon = 0$ show that there is no initial heat flow in the specimens coming from the loading plates. The high temperature in the background of the foams (pink colour) represents the surface temperature of the lens of the CCD camera used for DIC. Although there is no strain rate effect represented in the stress-strain behaviour, as expected from Eq. (1), the temperature increases with increasing strain rate, leading to the highest temperatures for the foams tested at a strain rate of $0.250\,s^{-1}$. The temperature increase in the thermographic images can be ascribed to high levels of plastic strain [35] similar to the deformation bands visualised in DIC. Due to the large thermal conductivity of the aluminium struts and the good thermal convection in the foams, there is no heat evolution visible for the foam investigated at the low strain rate of $0.025\,s^{-1}$. Hence, due to the fast heat transfer and convection, IR thermography is not suitable to study the deformation behaviour in Al foams under low strain rates, nevertheless, Fig. 3 gives the proof that IR thermography can be used for larger strain rates to track the propagation of the plastic deformation in foams. Similar to the previous results from DIC [12,25,42,43], there is a layer-wise propagation of the plastic deformation in form of a pronounced deformation band. In contrast to DIC, which provides only information from the specimen's surface, IR thermography outlines the heat evolution due to plastic deformation in the entire volume of the specimen.

The Ni/Al hybrid foams are characterised by a much larger heat evolution for equal strains and equal strain rates than the aluminium foams (see Fig. 4). The much larger heat evolution results from the higher energy absorption capacity of Ni/Al hybrid foams during plastic deformation of the Ni/Al hybrid foams compared to Al foams, which is expressed by the much larger area underneath the stress-strain curves. In addition, the larger energy absorption capacity is an effect of the local strengthening of each from strut by the nickel coating causing higher PCS and plateau stress. The maximal temperature of a foam before the experiment and during compression was determined for each foam and used to calculate the temperature changes $\Delta\theta$ as difference between the temperature in the foam for a specific strain state compared to the undeformed foam just before the experiment. Fig. 5 depicts the temperature changes $\Delta\theta$ expressed in degree Celsius for the Al and Ni/Al hybrid foams as function of strain rate and strain in order to gain a deeper understanding of the strain rate effect on the heat evolution during the compressive loading sequence and the effect of the nickel coating. The temperature in the Al foams increases with increasing plastic deformation (see Fig. 5 (a)), except for the lowest strain rate, which is affected by the large heat conduction. Further, there is a pronounced increase with increasing strain rate. For strains of $\varepsilon = 0.8$, the Al foam tested at a strain rate of $0.250\,s^{-1}$ provides a 2.5 times larger temperature change than the foam tested at an applied strain rate of $0.050\,s^{-1}$. Fig. 5 (c) and (d) represents an increasing temperature change with increasing nickel coating thickness. For a strain rate of $0.150\,s^{-1}$ and a deformation state corresponding to $\varepsilon \approx 0.35$, the temperature change increases by a factor of 2.5 from the Al foam to the Ni/Al hybrid foam with a coating thickness of 40 μm nickel and by a factor of about four for

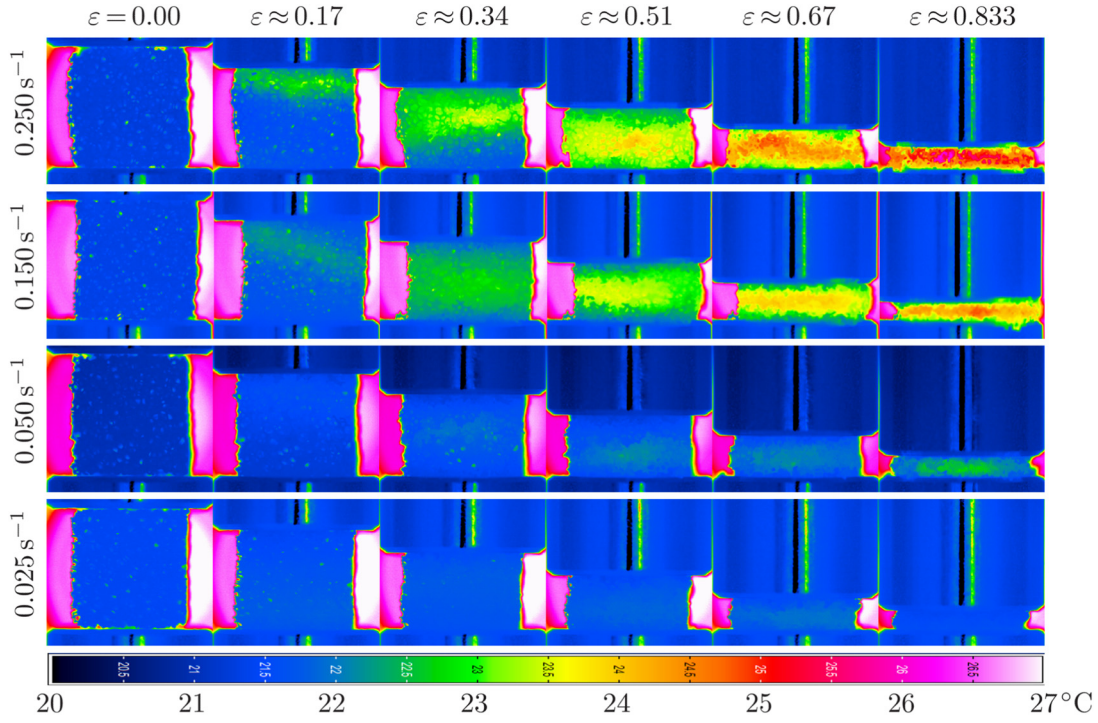

Fig. 3. Thermograms of the compressive loading sequence of Al foams for different strain rates.

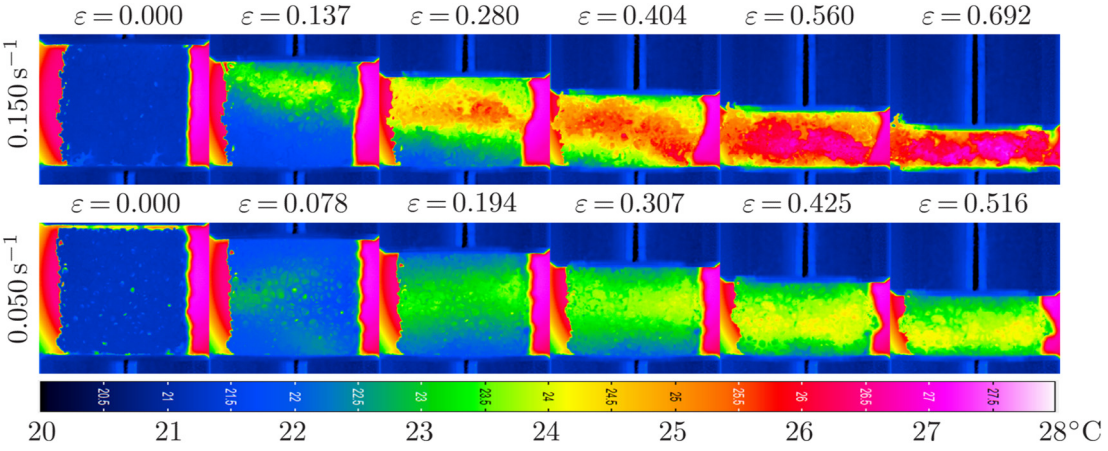

Fig. 4. Thermograms of the compressive loading sequence of Ni/Al hybrid foams (40 μm Ni) for different strain rates.

a coating thickness of 120 μm nickel. The increasing coating thickness results in an increasing strengthening effect and hence a larger energy absorption capacity of the corresponding Ni/Al hybrid foams, which is the reason for the larger heat evolution in the foams during compression. Furthermore, a comparison of Fig. 5 (b), (c) and (d) outlines an increase in the temperature change with increasing strain rate for the Ni/Al hybrid foams with a coating thickness of 120 μm similar to the Al foams.

3.2. Deformation analysis by thermography and DIC

In order to gain a deeper understanding of the plastic deformation in Al foams and Ni/Al hybrid foams a full thermomechanical analysis using a combination of DIC and IR thermography providing full-field strain and temperature information for the foams was performed. Since Crump et al. [44] only described the advantages of such a combination but did not realise it, the following results present such a

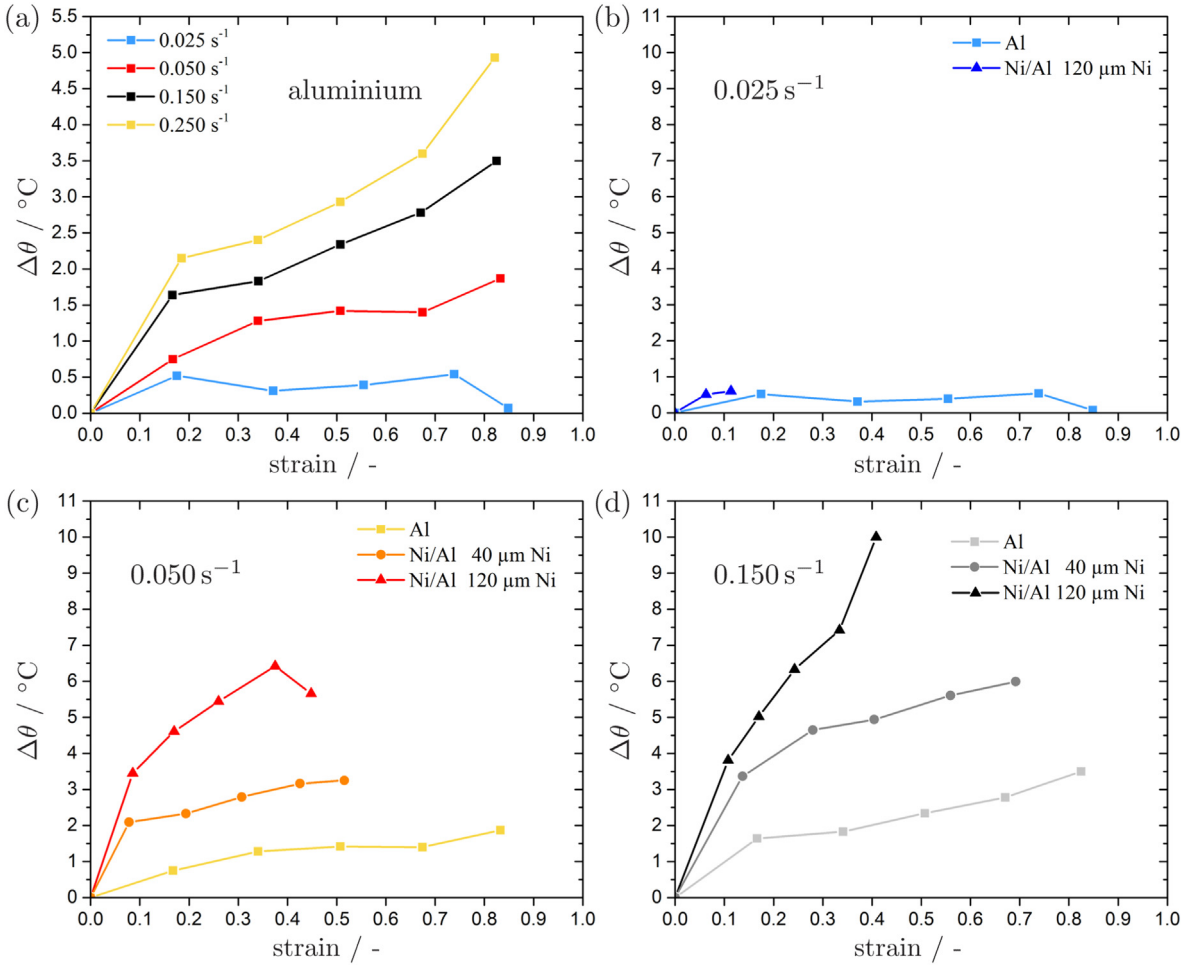

Fig. 5. Temperature change for Al foams and Ni/Al hybrid foams as function of global strain and strain rate: Al foams (a), 0.025 s^{-1} (b), 0.050 s^{-1} (c), 0.150 s^{-1} (d). (For a better comparison of the strain rate effect for the Al foams, there is a different vertical scale in Fig. 5(a) compared to Fig. 5(b)–(d)).

combination of DIC and IR thermography for metal foams, especially for Ni/Al hybrid foams for the first time.

Vesenjak et al. [34] revealed that IR thermography can be used to visualise plastification processes since plastic yielding is accompanied by heat dissipation. The larger the heat dissipation the more reliable are the results deduced from the thermograms. It was shown in the previous section that the Ni/Al hybrid foams with a coating thickness of 120 μm nickel provided the largest heat dissipation. Hence, these foams were used in the full thermomechanical analysis of the deformation behaviour. Fig. 6 compares directly the thermograms and the DIC images for a successive compressive deformation in Ni/Al hybrid foams with a coating thickness of 120 μm nickel. Since the DIC images and the thermograms were recorded from opposite sides of the foam, the DIC images were mirrored vertically for better comparison of the position and orientation of the localisation zones.

Fig. 6 depicts large deviations between the local temperature field and the local strain field. This is a consequence of the different physical measures. The temperature field obtained from IR thermography results from the heat energy dissipation in the entire volume of the foam specimens and is further affected by the thermal conductivity and the heat convection in the foam. In contrast, DIC measures strain only from the deformation of one surface of the foam. Deformation bands arising inside the foam or on the opposite side cannot be detected using only a single camera setup. Due to the necessary lighting for DIC, it is not possible to use 3D DIC with several cameras around the foam specimen in combination with IR thermography, since the lighting interferes with the acquisition of the temperature field by IR thermography. Also by using 3D DIC it is not possible to capture deformation inside the foams only on the entire outer surface. However, the strength of IR thermography is not quantifying strain, but providing a better understanding of the plastic yielding process in the entire specimen volume and tracing the plastification front [13]. Nevertheless, the main deformation area in both DIC images and IR thermograms comprises the same part of the specimen presenting a good qualitative correlation. The DIC images represent the total strain field including strains, which date back much longer than from the actual global strain. The thermographic images provide the actual areas of most plastic deformation activity. Deformation bands, which arise from lower global strain states provide lower temperatures than the actual deformation zone. However, both investigation methods exhibit a pore layer-wise collapse and deformation of the foams. Fig. 6 shows that for global strains of $\varepsilon = 0.260 - 0.375$, the highest temperatures arise on the right side of the specimen in mid-height. Since there is no deformation band in the strain field of the DIC images visible, the main plastic deformation for this global strain region does not take place on the specimen surface facing the CCD camera but somewhere else in the volume.

Fig. 7 traces the temperature and the local strain ε_{yy} in the vertical centre line across the foam of Fig. 6 for successive compression loading showing a good qualitative correlation. The maximal temperature increases with increasing global strain and the width of the plastification zone, which is characterised by heat energy dissipation increases as well. A similar behaviour can be seen for the distribution of local strains. They increase with increasing global strain and the width of the deformation zone becomes larger.

However, due to the different physical measures, there is no direct correlation between DIC and IR thermography. The thermograms present only one deformation zone, while the DIC images as well as Fig. 7 show two distinct deformation bands. This deviation results from heat conductivity making it impossible to distinguish several adjacent deformation bands by IR thermography, at least in this low strain rate regime.

4. Conclusion

The present contribution dealt with a full thermomechanical analysis including strain rate effects of Al foams and Ni/Al hybrid foams by a combination of DIC and IR thermography. The contribution goes beyond the state-of-the-art since for the first time, such a full-field thermomechanical deformation analysis providing full-field strain and temperature information for an indirect visualisation of irreversible deformation and plastification was performed for metal foams. There were no strain rate effects on the stress-strain response in the investigated low strain rate regime. However, there were pronounced strain rate effects regarding the heat energy dissipation during plastic deformation. Increasing strain rates lead to increasing temperatures in the specimens. The heat evolution in Ni/Al hybrid foams is larger than in Al foams as a result of lower conductivity and higher plastic dissipation. The maximal temperature increase is up to 31 °C for Ni/Al hybrid foams with a coating thickness of 120 μm. Due to the low heat evolution in the Al foams under lower strain rates, IR thermography is only conditionally applicable to Al foams in this strain rate regime. However, based on the much larger plastic dissipation, IR thermography even in combination with DIC can be advantageously used for Ni/Al hybrid foams especially with increasing coating thickness.

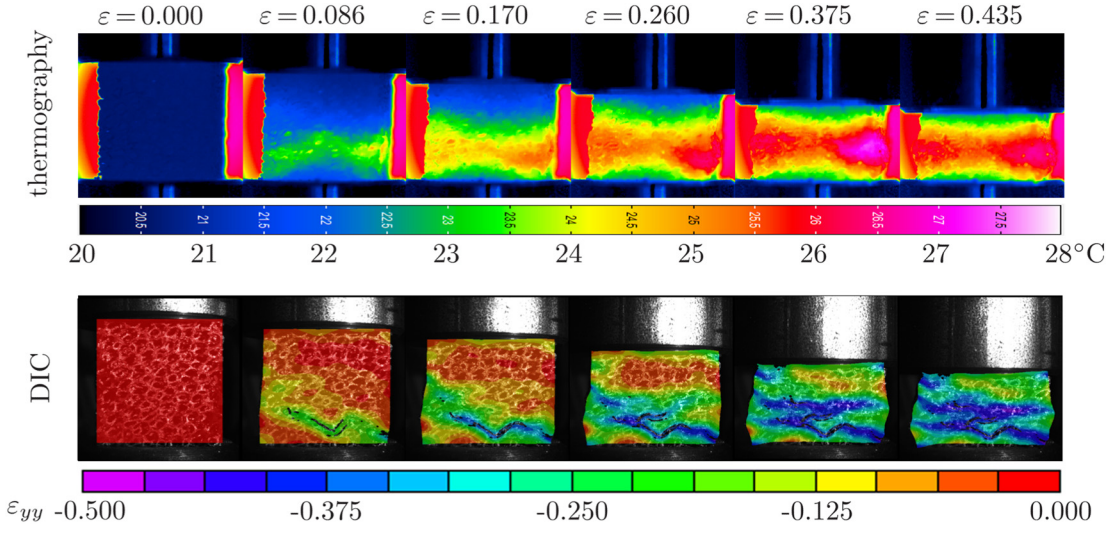

Fig. 6. Comparison of IR thermography and DIC for observation of the successive deformation of a Ni/Al hybrid foam with 120 μm Ni at a strain rate of 0.050 s^{-1}.

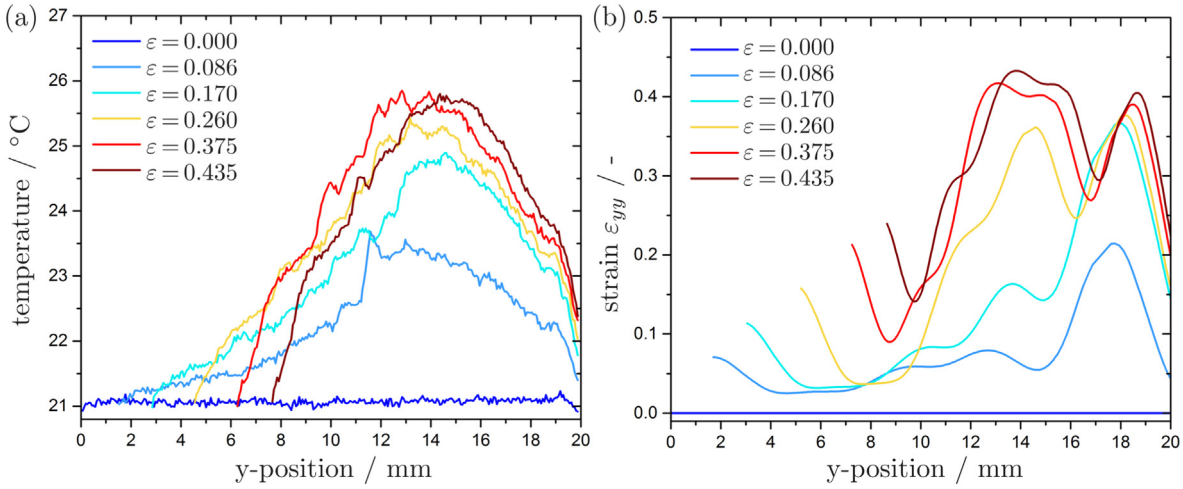

Fig. 7. Evolution of the deformation bands described by the temperature obtained from the thermograms (a) and by the local strains from the DIC images (b) for a vertical centre line of the foam in Fig. 6.

The direct comparison of the results from DIC and IR thermography depicts deviations between temperature and strain field as consequence of the different physical measures. The temperature field results from the heat energy dissipation due to plastic deformation in the entire volume of the foam and is influenced by the thermal conductivity and the heat convection in the foam. In contrast, the local strain field from DIC only describes the deformation of the foam's surface. Krstulović-Opara et al. [13] stated that the strength of IR thermography is not a quantifying strain, but providing a better understanding of the plastic yielding process in the entire specimen volume and tracing the plastification front. DIC and IR thermography differ in the time scale on which information about the plastic deformation process is given. While DIC images present the total strain history, the IR thermograms provide the actual areas of most plastic deformation in the entire volume of the specimens. The heat of previous deformations cools down due to heat convection and conduction. Hence, the hottest area represents the actual deformation zones.

The larger the heat dissipation the more reliable are the results deduced from IR thermography. Hence, IR thermography is very suitable for the investigation of the deformation phenomena of metal foams under large strain rates. Based on the much larger heat evolution, IR thermography is more suitable for the investigation of Ni/Al hybrid foams than for Al foams, even under low strain rates. The strain rate dependent material behaviour can be investigated by synchronised measurement of strain fields via DIC and temperature distributions via IR thermography. Hence, summing up the advantages of both methods, DIC and IR thermography, the coupling of DIC with IR thermography is a very powerful method for the analysis of cellular materials used as crash absorbers especially in high impact testing. Furthermore, based on the investigations in this work a thermomechanically coupled material model of Ni/Al hybrid forms can be developed to predict energy absorption characteristics and plastic deformation behaviour of these structures in the future.

Author statement

Anne Jung: Conceptualization, methodology, validation, investigation, resources, data curation, supervision, writing - original draft, writing - review & editing, project administration, funding acquisition

Stefan Bronder: Investigation, validation, formal analysis

Stefan Diebels: Conceptualization, supervision

Marvin Schmidt: Conceptualization, methodology, validation, investigation, writing - original draft

Stefan Seelecke: Conceptualization, supervision

Acknowledgements

The authors gratefully acknowledge the Daimler and Benz Foundation (project number 32-07/14) for financial support.

References

[1] T.A. Schaedler, W.B. Carter, Architected cellular materials, Annu. Rev. Mater. Res. 46 (2016) 187–210.
[2] F. García-Moreno, Commercial applications of metal foams: their properties and production, Materials 9 (2) (2016) 85.
[3] S.F. Fischer, Energy absorption efficiency of open-cell pure aluminum foams, Mater. Lett. 184 (2016) 208–210.
[4] B. Bouwhuis, J. McCrea, G. Palumbo, G. Hibbard, Mechanical properties of hybrid nanocrystalline metal foams, Acta Mater. 57 (14) (2009) 4046–4053.
[5] C. Devivier, V. Tagliaferri, F. Trovalusci, N. Ucciardello, Mechanical characterization of open cell aluminium foams reinforced by nickel electro-deposition, Mater. Des. 86 (2015) 272–278.
[6] A. Jung, Z. Chen, J. Schmauch, C. Motz, S. Diebels, Micromechanical characterisation of Ni/Al hybrid foams by nano- and microindentation coupled with EBSD, Acta Mater. 102 (2016) 38–48.
[7] A. Jung, S. Diebels, A. Koblischka-Veneva, J. Schmauch, A. Barnoush, M.R. Koblischka, Microstructural analysis of electrochemical coated open-cell metal foams by EBSD and nanoindentation, Adv. Eng. Mater. 16 (1) (2014) 15–20. https://doi.org/10.1002/adem.201300187.
[8] A. Jung, H. Natter, S. Diebels, E. Lach, R. Hempelmann, Nanonickel coated aluminum foam for enhanced impact energy absorption, Adv. Eng. Mater. 13 (1-2) (2011) 23–28. https://doi.org/10.1002/adem.201000190.
[9] A. Antenucci, S. Guarino, V. Tagliaferri, N. Ucciardello, Improvement of the mechanical and thermal characteristics of open cell aluminum foams by the electrodeposition of Cu, Mater. Des. 59 (2014) 124–129.
[10] Y. Sun, R. Burgueño, W. Wang, I. Lee, Modeling and simulation of the quasi-static compressive behavior of Al/Cu hybrid open-cell foams, Int. J. Solids Struct. 54 (2015) 135–146.
[11] W. Wang, R. Burgueño, J.-W. Hong, I. Lee, Nano-deposition on 3-D open-cell aluminum foam materials for improved energy absorption capacity, Mater. Sci. Eng. A 572 (2013) 75–82.
[12] A. Jung, S. Diebels, Synthesis and mechanical properties of novel Ni/PU hybrid foams: a new economic composite material for energy absorbers, Adv. Eng. Mater. 18 (4) (2016) 532–541.
[13] L. Krstulović-Opara, M. Surjak, M. Vesenjak, Z. Tonković, J. Kodvanj, ž. Domazet, Comparison of infrared and 3D digital image correlation techniques applied for mechanical testing of materials, Infrared Phys. Technol. 73 (2015) 166–174.
[14] O. Breitenstein, W. Warta, M. Langenkamp, Lock-in Thermography: Basics and Use for Evaluating Electronic Devices and Materials, vol. 10. Springer Science & Business Media. 2010.
[15] M. Dolce, D. Cardone, Mechanical behaviour of shape memory alloys for seismic applications 1. Martensite and austenite NiTi bars subjected to torsion, Int. J. Mech. Sci. 43 (11) (2001) 2631–2656.

[16] M. Dolce, D. Cardone, Mechanical behaviour of shape memory alloys for seismic applications 2. Austenite NiTi wires subjected to tension, Int. J. Mech. Sci. 43 (11) (2001) 2657–2677.
[17] M. Schmidt, A. Schütze, S. Seelecke, Elastocaloric cooling processes: the influence of material strain and strain rate on efficiency and temperature span, APL Mater. 4 (6) (2016) 064107.
[18] M. Schmidt, J. Ullrich, A. Wieczorek, J. Frenzel, A. Schütze, G. Eggeler, S. Seelecke, Thermal stabilization of NiTiCuV shape memory alloys: observations during elastocaloric training, Shape Mem. Superelast. 1 (2) (2015) 132–141.
[19] T. Lehmann, et al. On a generalized constitutive law for finite deformations in thermo-plasticity and thermo-viscoplasticity, in: C.S. Desai (Ed.), Constitutive laws for engineering materials, Theory and Applications, Elsevier, New York, 1987, pp. 173–184.
[20] Z. Tonković, J. Sorić, W.B. Krätzig, On nonisothermal elastoplastic analysis of shell components employing realistic hardening responses, Int. J. Solids Struct. 38 (28) (2001) 5019–5039.
[21] A. Veteleanu, Research concerning the influence of the artificial aging treatment over the mechanical characteristics of composite materials with a metallic matrix, Metalurgia 63 (6) (2011) 45–50.
[22] T. Farrell, D. Greig, The thermal conductivity of nickel and its alloys, J. Phys. C Solid State Phys. 2 (8) (1969) 1465.
[23] R. Powell, R. Tye, M. Hickman, The thermal conductivity of nickel, Int. J. Heat Mass Transf. 8 (5) (1965) 679–688.
[24] D. Wagner, N. Ranc, C. Bathias, P. Paris, Fatigue crack initiation detection by an infrared thermography method, Fatigue Fract. Eng. Mater. Struct. 33 (1) (2010) 12–21.
[25] A. Jung, A.D. Pullen, W.G. Proud, Strain-rate effects in Ni/Al composite metal foams from quasi-static to low-velocity impact behaviour, Compos. A: Appl. Sci. Manuf. 85 (2016) 1–11.
[26] B. Koohbor, A. Kidane, W.-Y. Lu, Characterizing the constitutive response and energy absorption of rigid polymeric foams subjected to intermediate-velocity impact, Polym. Test. 54 (2016) 48–58. http://www.sciencedirect.com/science/article/pii/S0142941816304755. https://doi.org/10.1016/j.polymertesting.2016.06.023.
[27] S. Ravindran, B. Koohbor, P. Malchow, A. Kidane, Experimental characterization of compaction wave propagation in cellular polymers, Int. J. Solids Struct. 139-140 (2018) 270–282. http://www.sciencedirect.com/science/article/pii/S0020768318300507. https://doi.org/10.1016/j.ijsolstr.2018.02.003.
[28] B.-C. Chang, J.A. Shaw, M.A. Iadicola, Thermodynamics of shape memory alloy wire: modeling, experiments, and application, Contin. Mech. Thermodyn. 18 (1-2) (2006) 83–118.
[29] F. Welsch, J. Ullrich, H. Ossmer, M. Schmidt, M. Kohl, C. Chluba, E. Quandt, A. Schütze, S. Seelecke, Numerical simulation and experimental investigation of the elastocaloric cooling effect in sputter-deposited TiNiCuCo thin films, Contin. Mech. Thermodyn. (2017) 1–16.
[30] E. Solórzano, F. Garcia-Moreno, N. Babcsán, J. Banhart, Thermographic monitoring of aluminium foaming process, J. Nondestruct. Eval. 28 (3-4) (2009) 141–148.
[31] W. Clarke, R. Mack, Void detection in polyurethane foam using thermographic imaging, J. Cell. Plast. 22 (5) (1986) 404–414.
[32] V. Crupi, G. Epasto, E. Guglielmino, Low-velocity impact strength of sandwich materials, J. Sandw. Struct. Mater. 13 (4) (2011) 409–426.
[33] W. Wang, J. Dulieu-Barton, O. Thomsen, A methodology for characterizing the interfacial fracture toughness of sandwich structures using high speed infrared thermography, Exp. Mech. 56 (2016) 121–132.
[34] M. Vesenjak, L. Krstulović-Opara, Z. Ren, Characterization of irregular open–cell cellular structure with silicone pore filler, Polym. Test. 32 (8) (2013) 1538–1544.
[35] M. Vesenjak, M.A. Sulong, L. Krstulović-Opara, M. Borovinšek, V. Mathier, T. Fiedler, Dynamic compression of aluminium foam derived from infiltration casting of salt dough, Mech. Mater. 93 (2016) 96–108.
[36] I. Duarte, M. Vesenjak, L. Krstulović-Opara, Dynamic and quasi-static bending behaviour of thin-walled aluminium tubes filled with aluminium foam, Comput. Struct. 109 (2014) 48–56.
[37] I. Duarte, M. Vesenjak, L. Krstulović-Opara, I. Anžel, J.M. Ferreira, Manufacturing and bending behaviour of in situ foam-filled aluminium alloy tubes, Mater. Des. 66 (2015) 532–544.
[38] I. Duarte, M. Vesenjak, L. Krstulović-Opara, Z. Ren, Static and dynamic axial crush performance of in-situ foam-filled tubes, Compos. Struct. 124 (2015) 128–139.
[39] L. Krstulović-Opara, M. Vesenjak, I. Duarte, Z. Ren, ž. Domazet, Infrared thermography as a method for energy absorption evaluation of metal foams, Mater. Today Proc. 3 (4) (2016) 1025–1030.
[40] S. Heinze, Z. Chen, A. Jung, S. Diebels, A. Düster, Numerical analysis of Ni/Al hybrid metal foams using the finite cell method, PAMM · Proc. Appl. Math. Mech. 15 (2015) 299–300.
[41] B. Koohbor, S. Ravindran, A. Kidane, Effects of cell-wall instability and local failure on the response of closed-cell polymeric foams subjected to dynamic loading, Mech. Mater. 116 (2018) 67–76. (iUTAM Symposium on Dynamic Instabilities in Solids). http://www.sciencedirect.com/science/article/pii/S0167663616304458. https://doi.org/10.1016/j.mechmat.2017.03.017.
[42] A. Bastawros, R. McManuis, Case study: use of digital image analysis software to measure non-uniform deformation in cellular aluminum alloys, Comput. Stand. Interfaces 20 (6) (1999) 459–460.
[43] A. Jung, S. Diebels, Microstructural characterisation and experimental determination of a multiaxial yield surface for open-cell aluminium foams, Mater. Des. 131 (2017) 252–264.
[44] D. Crump, J. Dulieu-Barton, R. Fruehmann, Challenges in synchronising high speed full-field temperature and strain measurement, Thermomechanics and Infra-Red Imaging, vol. 7, Springer. 2011, pp. 1–7.